Photoionization of $5d$ and $4f$ subshells of high-Z elements

B. R. Tambe
Department of Chemistry and Physics, Southern Technical Institute, Marietta, Georgia 30060

Steven T. Manson
Department of Physics and Astronomy, Georgia State University, Atlanta, Georgia 30303
(Received 22 December 1983)

Calculations of the photoionization of $5d$ and $4f$ subshells of a number of heavy elements have been performed with use of relativistic Dirac-Slater wave functions. Cross sections, branching ratios, and photoelectron angular distributions have been obtained and their systematics explored as a function of Z. The extent of the relativistic splitting of the zeros in the $5d \rightarrow \epsilon f$ dipole matrix elements has been investigated and the implications have been discussed. Comparisons with existing experiment and more sophisticated theory (Dirac-Fock, relativistic random-phase approximation) have been made, and the agreement was generally good.

I. INTRODUCTION

Recent advances in experimental photoelectron spectroscopy have made it increasingly possible to make reliable measurements of the details of the photoionization process. In particular, it is now possible to study the effects of relatively small interactions. In the light of this development, we have undertaken a broad theoretical study of photoionization within a relativistic framework. In this paper we report the results of our studies of the $4f$ and $5d$ subshells of the heavy elements. The photoionization of the $5d$ subshell of mercury has been studied experimentally[1-5] and the $4f$ of Hg has also been studied.[5] It is, therefore, possible to gain some insight into the accuracy of our theoretical results *via* comparison with experiment.

The heavy elements differ most markedly from the light elements in the strength of the relativistic interactions. The theoretical methods to perform realistic calculations have been described and tested in several recent papers.[6-8] The framework for a systematic survey of the heavy elements has thus been established. Among the experimentally measurable quantities which describe the photoionization of a given subshell are photoionization cross section (σ), photoelectron angular distribution asymmetry parameter (β), and branching ratio (γ). The branching ratio arises from the relativistic splitting of a given nl subshell into a $j=l+\frac{1}{2}$ component and $j=l-\frac{1}{2}$ component due to the spin-orbit interaction. In certain cases, the splitting of thresholds alone explains the behavior of the branching ratio. However, it has recently been shown in the case of the $5d$ subshell of mercury[7] that the photoionization cross sections for the two components have different shapes. The dynamical effects giving rise to these differences are, of course, explicitly relativistic. Hence the branching ratio in this case can be understood only through an explicitly relativistic calculation.

The asymmetry parameter β, on the other hand, can be calculated in a relativistic as well as a nonrelativistic approximation. In the relativistic treatment the asymmetry parameters corresponding to the two spin-orbit components of a given nl subshell differ from each other for a number of reasons. Most important are the relativistic dynamical effects that lead to differing matrix elements and phase shifts for the two components. It is also known that the presence of a Cooper minimum affects the shape of the asymmetry parameter curve. Further, it has been shown recently that the positions of these Cooper minima can change greatly when relativistic interactions are included in the calculation.[8,9] Thus it seems reasonable to expect significant effects of relativistic interactions. The shift in the position of the Cooper minima also strongly affects the cross sections.

In view of these results, we expect a systematic relativistic study to reveal the features of the photoionization of heavy elements. Another reason for restricting our study to high-Z elements is that the j-j coupling scheme is known to be valid for these elements. This coupling scheme is implicit in the solution of Dirac equations. For lower-Z elements this scheme begins to break down and the agreement with experiment is no longer very good.[7]

In this paper we report our results for the $4f$ and $5d$ subshells of a series of heavy elements. Of these we have studied a few more extensively than others. These are tungsten ($Z=74$), for which the $5d$ subshell is not completely filled, mercury ($Z=80$), which is a closed subshell atom and which has also been studied experimentally,[1-5] and uranium ($Z=92$), which is a transition element in which the $5f$ subshell is already bound which greatly affects the $nd \rightarrow \epsilon f$ oscillator strengths.

The theoretical formulation used was discussed in Ref. 7 in some detail where relativistic calculations of the photoionization of Hg and Cd were presented. In these calculations relativistic effects are explicitly included by using the Dirac equation. The atomic potential used in these equations is, however, approximate. In one standard approximation the exchange interaction is included *via* a Slater-type central field. This approximation is referred to as the Dirac-Slater (DS) approximation. The nonrelativistic counterpart of this approximation is the Hartree-Slater (HS) approximation.[10] In a more accurate approximation, the exchange interaction is included explicitly

self-consistently through a nonlocal exchange potential. This leads to a much more complicated numerical problem. This approximation is the relativistic analog of the Hartree-Fock (HF) approximation[10] and hence it is generally referred to as the Dirac-Fock (DF) approximation. Implicit in both of these formulations are one-particle orbitals. It was shown in Ref. 7 that the DS approximation leads to satisfactory agreement between theory and experiment for the $5d$ branching ratio of mercury. It also explained the qualitative features of the cross-section curves quite well. However, the peak of the cross section is shifted toward the threshold and the peak is higher than the experimental value. Hence one must resort to the DF approximation to obtain reliable absolute cross sections. We will discuss the validity of the DS approximation for the asymmetry parameter at a later point in this paper. It will be shown that the DS approximation leads to satisfactory agreement with the experiment for the asymmetry parameter also. In view of these results and the simplicity of DS calculations as compared to DF calculations, the DS approximation presents itself as an attractive approach for studying the systematics in the photoionization of heavy elements.

II. THEORY AND METHOD OF CALCULATION

The wave functions of the bound orbitals and the potential used in the calculation of continuum orbitals are obtained from the computer code of Lieberman *et al.*[11] The continuum wave function is calculated by solving the two coupled first-order equations[6] by using this same potential. The continuum wave function consists of a major (P) and a minor (Q) component normalized so that

$$\left.\begin{matrix}P(r)\\Q(r)\end{matrix}\right\}\rightarrow\left[\frac{E\pm c^2}{2E}\right]^{1/2}\times\left\{\begin{matrix}\cos\\\sin\end{matrix}\right\}\left[kr+\frac{E}{kc^2}\ln(2kr)-(l+1)\frac{\pi}{2}+\xi_c+\delta_{j_\alpha}\right], \quad (1)$$

where E is the total energy ($E>mc^2$), ξ_c is the relativistic Coulomb phase shift, and δ_{j_α} is the non-Coulomb phase shift.

The relativistic cross section for photoionization of a bound electron with angular momentum j_β by electric dipole radiation is given by[6]

$$\sigma=\frac{4\pi c}{k\omega}\left[\frac{2j_\beta-1}{12j-1}|R_{j_\beta}-1|^2+\frac{1}{12j_\beta(j_\beta+1)}|R_{j_\beta}|^2+\frac{2j_\beta+3}{12(j+1)}|R_{j_\beta}+1|\right], \quad (2)$$

with ω the photon energy and $k=(E^2-c^4)^{1/2}$ all in a.u. The matrix elements R_{j_α} are calculated in the Coulomb gauge (which reduces to the velocity form in the nonrelativistic limit). In this gauge

$$R_{j_\alpha}=\frac{i}{\sqrt{2}}[(\kappa_\alpha-\kappa_\beta)(I_2^+-I_0^+)+2I_2^++I_0^-]e^{i\xi_{j_\alpha}}, \quad (3)$$

where α and β refer to continuum and bound states and κ is $-l-1$ for $j=l+\frac{1}{2}$ and $+l$ for $j=l-\frac{1}{2}$. The phase involved in this expression is $\xi_{j_\alpha}=\xi_c+\delta_{j_\alpha}$ and

$$I_L^\pm=\int_0^\infty(P_\alpha Q_\beta\pm Q_\alpha P_\beta)j_L(\omega r/c)dr, \quad (4)$$

where the j_L are spherical Bessel functions.

The angular distribution of photoelectrons from unpolarized targets in an electric dipole photoionization process is given by[12]

$$\frac{d\sigma}{d\Omega}=\frac{\sigma}{4\pi}[1+\beta P_2(\cos\theta)], \quad (5)$$

where P_2 is the Legendre polynomial of second order and θ is the angle between photon polarization and photoelectron directions. For unpolarized photons $\beta\rightarrow-\frac{1}{2}\beta$ and θ is the angle between photon and photoelectron directions. β can vary between -1 and 2 only which ensures that the differential cross section is always positive.

The angular distribution asymmetry parameter is given by[6]

$$\beta=\mathscr{D}^{-1}\left[\frac{(2j-3)(2j-1)}{48j^2}|R_{j-1}|^2-\frac{(2j-1)(2j+3)}{48j^2(j+1)^2}|R_j|^2+\frac{(2j+3)(2j+5)}{48(j+1)^2}|R_{j+1}|^2\pm\frac{(2j-1)}{8j^2(j+1)}\mathrm{Re}(R_jR_{j-1}^*)\pm\frac{(2j+3)}{8j(j+1)^2}\mathrm{Re}(R_jR_{j+1}^*)-\frac{(2j-1)(2j+3)}{8j(j+1)}\mathrm{Re}(R_{j-1}R_{j+1}^*)\right], \quad (6)$$

where

$$\mathscr{D}=\frac{(2j-1)}{12j}|R_{j-1}|^2+\frac{1}{12j(j+1)}|R_j|^2+\frac{2j+3}{12(j+1)}|R_{j+1}|^2$$

where Re is real part, upper sign for $j=l+\frac{1}{2}$ and lower sign for $j=l-\frac{1}{2}$.

The third physical quantity of interest is the branching ratio. This is the ratio of the photoionization cross sections for the $j=l+\frac{1}{2}$ and $j=l-\frac{1}{2}$ orbitals. This ratio deviates from the ratio of the occupation numbers (i.e., the statistical ratio) for reasons discussed previously.

In an actual DS calculation for the dipole matrix element one must also choose between a relaxed ion core with an ionic bound state and an unrelaxed ion core with an atomic bound state. Walker and Weber[6] have chosen the former. The ionic bound state is more compact than the atomic bound state. This results in the peak in the cross section curve being higher and shifting closer to the threshold. Keller and Combet Farnoux[13] have pointed out that the results of Ref. 6 can be improved through a

HF calculation. It is shown in Ref. 7 that part of the disagreement is due to the use of the ionic bound state and better agreement with experiment can be obtained within the DS framework by using an atomic bound state and the potential corresponding to an unrelaxed ion core. The results can be improved further in a DF calculation which used relaxed ion core potential and an atomic bound state.[7] We restrict ourselves to a simpler DS calculation using atomic bound states and an unrelaxed ion core. The continuum orbital so obtained was used to calculate the dipole matrix elements needed to calculate σ, β, and γ.

III. RESULTS AND DISCUSSION

The validity of the DS approximation for calculating cross sections and branching ratios has been discussed in Ref. 7. The conclusion drawn from this discussion has been mentioned in the first two sections. So far we have not discussed the results obtained for β from a DS calculation. In Fig. 1 a comparison of β obtained from a DS and a DF calculation for $5d_{3/2}$ subshell of Hg is shown. Our DF calculation yields excellent agreement with experiment for cross sections and branching ratios.[7] It is shown in Ref. 7 that there is some disagreement between the values of σ obtained in the two calculations but the agreement in the values of β in the two calculations is quite good.[4] This can be understood quite easily. While σ depends upon the absolute magnitudes of the dipole matrix elements, β is determined by the relative magnitudes of these elements and the phase shifts associated with the continuum wave functions. Since the DS approximation yields good results for the branching ratio γ, the relative magnitudes of the various matrix elements and their energy dependence can be expected to be accurate in this calculation. In Fig. 2 calculated phase shifts for the continuum functions obtained from these two approximations relevant to the photoionization of Hg $5d$ are given. The overall agreement between the DS and DF approximations is seen to be good. The phase shifts in the DF calculation are somewhat larger at low energy and slightly lower at higher energy. The differences are not great, however, which gives us confidence in the DS results. As a further test of the DS calculation we compare our theoretical results with experimental data. Fortunately, a considerable amount of experimental data is now available for the asymmetry parameter of the $5d$ subshell of mercury. In Figs. 3 and 4 we compare this experimental data [4,5,14,15] with our theoretical DS results. The agreement in the threshold region shown in Fig. 3 between theory and experiment is quite good for both $5d_{3/2}$ and $5d_{5/2}$. In Fig. 4, which shows higher energies where the spin-orbit doublet is not resolved, we find excellent agreement. Note that, surprisingly, our DS calculation does better than the relativistic random-phase approximation[16] (RRPA) (not shown) near the Cooper minimum, but this must be considered fortuitous. This is a good test not only for our asymmetry parameter but also for the location of the Cooper minimum.

We conclude that the DS approximation may be applied to gain an understanding of the various features of

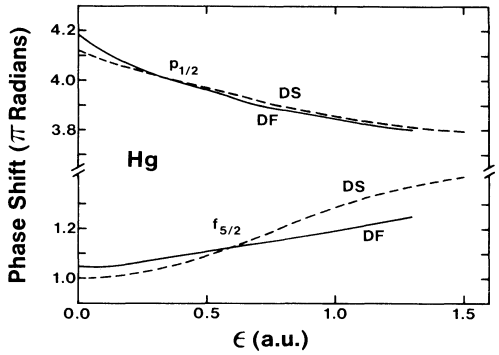

FIG. 2. Phase shifts of the $p_{1/2}$ and $f_{5/2}$ continuum arising from $5d_{3/2}$ photoionization in Hg; comparison of the present DS results and the DF results of Ref. 7.

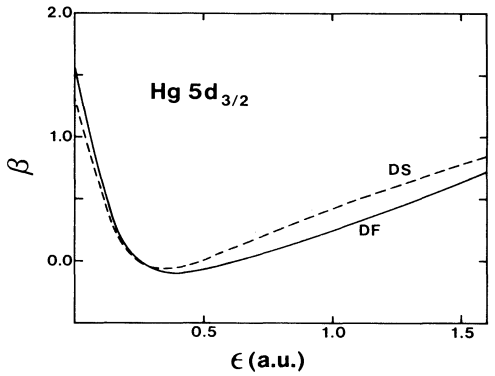

FIG. 1. Photoelectron angular distribution asymmetry parameter β for Hg $5d_{3/2}$ in the threshold region; comparison between the present DS results and the DF results of Ref. 7.

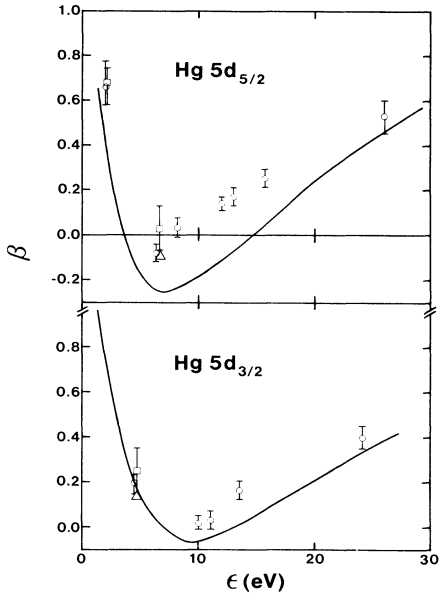

FIG. 3. Photoelectron angular distribution asymmetry parameter for Hg $5d_{3/2}$ and $5d_{5/2}$ in the threshold region; comparison of the theoretical DS results with the experimental results of Ref. 4 (circles), Ref. 5, (squares), and Ref. 14 (triangles).

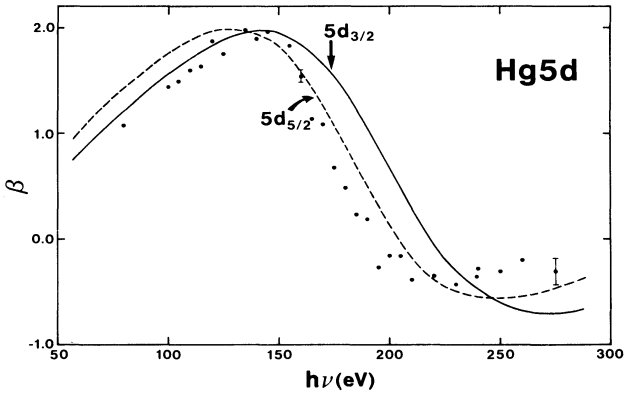

FIG. 4. Photoelectron angular distribution asymmetry parameter for Hg $5d_{3/2}$ and $5d_{5/2}$; comparison of the present DS results with the unresolved $5d$ results of Ref. 5.

photoionization of heavy elements. In what follows we discuss the photoionization of $4f$ and $5d$ subshells of heavy elements.

A. Phase shifts

The various physical quantities which characterize photoionization are determined by the dipole matrix element and the phase shifts of the continuum functions. The dipole matrix element itself is also indirectly dependent upon the phase shifts. It is, therefore, instructive to discuss the phase shifts of the continuum functions before proceeding to a discussion of cross sections, asymmetry parameters, and branching ratios.

Phase shifts for the g and d continuum functions arising in $4f$ photoionization are shown in Figs. 5 and 6, respectively, for several cases; both nonrelativistic

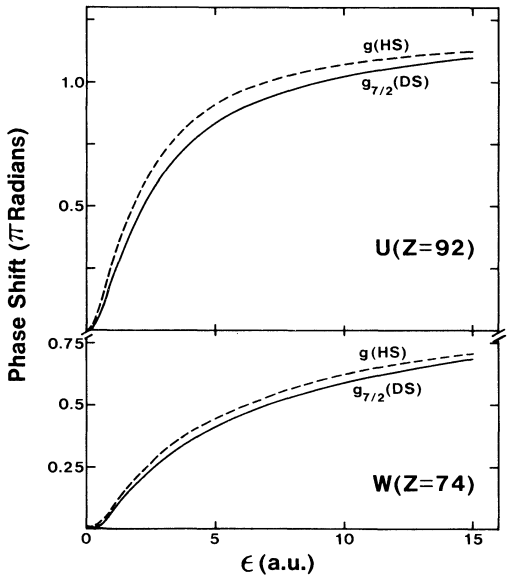

FIG. 5. Phase shifts, in units of π radians, of $g_{7/2}$ continua for W ($Z=74$) and U ($Z=92$) which arise in $4f$ photoionization. The solid curves are the present DS results and the dashed curves are the HS results for the nonrelativistic g continua.

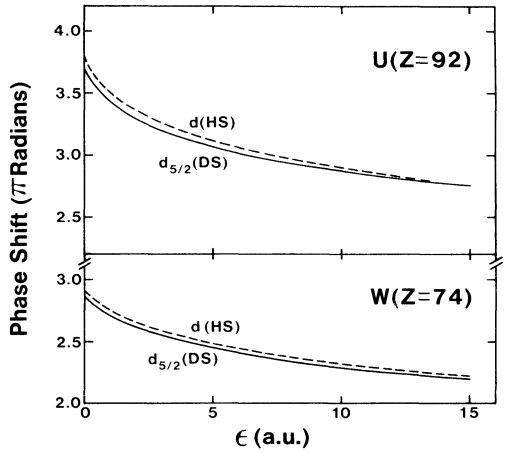

FIG. 6. Phase shifts, in units of π radians, of $d_{5/2}$ continua for W ($Z=74$) and U ($Z=92$) which arise in $4f$ photoionization. The solid curves are the present DS results and the dashed curves are the HS results for the nonrelativistic d continua.

Hartree-Slater[17] (HS) and our DS results are shown. It is seen in Fig. 5 for tungsten ($Z=76$) and uranium ($Z=92$) that δ_g is virtually zero at threshold in both approximations. This is a result of the huge angular momentum (centrifugal) barrier seen by g waves which keeps the wave function from having any appreciable amplitude in the inner region where the potential is nonhydrogenic. With increasing energy, however, the g wave can penetrate and a broad shape resonance ensues. That the shape resonance gets narrower, with increasing Z, is a consequence of the increasing strength of the electrostatic attraction.

Only $\delta_{g_{7/2}}$ is shown in Fig. 5 but $\delta_{g_{9/2}}$ lies slightly below $\delta_{g_{7/2}}$ and is almost parallel to it, in all cases. The fact that $\delta_{g_{7/2}} > \delta_{g_{9/2}}$ is a special case of a general phenomenon; it is due to the fact that the spin-orbit interaction is attractive for $j = l - \frac{1}{2}$ states and repulsive for $j = l + \frac{1}{2}$ states. The difference between the phase shifts of the spin-orbit doublets increases with Z owing to the increase of the strength of the spin-orbit interaction with Z.

Note further, from Fig. 5, that the nonrelativistic δ_g is always greater than either of the relativistic, $\delta_{g_{7/2}}$ being the larger of the relativistic as discussed above. They can be compared directly because the low-energy Coulomb phase shifts differ by a negligible amount, of order α^2, since we are dealing with continuum electrons in an asymptotic field of unit charge.[18] Thus the net nonrelativistic potential is more attractive for g waves than either of the relativistic potentials. The effect of relativistic interactions is, therefore, to expand the relativistic g-wave function; this is in contrast to the result for the hydrogen atom where all wave functions, discrete and continuum, *contract* under the influence of relativistic interactions.[19] Relativistic interactions are largest near the nucleus; thus the contraction effect is greatest for s states, which have the largest amplitude near the nucleus, and gets successively smaller with increasing angular momentum. For multielectron atoms the contraction occurs for the orbital

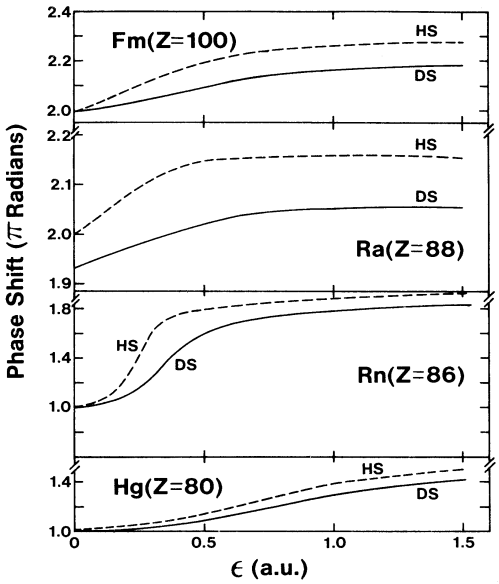

FIG. 7. Phase shifts, in units of π radians, of $f_{5/2}$ continua for Hg ($Z=80$), Rn ($Z=86$), Ra ($Z=88$), and Fm ($Z=100$) which arise in $5d$ photoionization. The solid curves are the present DS results and the dashed curves are the HS results for the nonrelativistic f continuum.

$1s$ through $3d$. This causes the nucleus to be screened more effectively by the inner subshells making the net electrostatic field less attractive in the outer part of the atom. The outer subshells, and continuum orbitals, respond to this combination of effects which act in opposite directions. The higher s and p orbitals, which have significant amplitude near the nucleus still contract, while the higher $l \geq 2$ orbitals, which are small near the nucleus, expand. This is the reason for the expansion of the relativistic continuum g-wave functions compared to nonrelativistic. This matter is discussed in detail elsewhere for Hg.[19]

These ideas are confirmed further in Fig. 6 for the d-wave phase shifts where it is seen that the nonrelativistic phase shift is greater than the relativistic. The systematics of the relativistic d-wave phase shifts are the same as the nonrelativistic which are discussed elsewhere.[20]

The phase shifts for continuum f- and p-waves, which result from $5d$ photoionization, are shown in Figs. 7 and 8, respectively. The results for δ_f (Fig. 7) shows threshold values of about 1 (in units of π) for $Z \leq 86$ and about 2 for $Z \geq 88$, indicating that the potential is sufficiently strong to bind a second f state in the ground state for the higher Z's; the effective f-wave potential is a double-welled potential separated by a barrier and the $5f$ is now bound in the inner well. There is also a shape resonance for $Z=86$ which is broader in the relativistic calculation indicating that the barrier separating the two potential wells broadens relativistically. The systematics of the nonrelativistic δ_f and the relativistic $\delta_{f_{5/2}}$ (the larger of the relativistic δ_f's) are quite similar.[20] In all the cases, the nonrelativistic δ_f is greater than either of the relativistic for reasons discussed above. The p-wave phase shifts (Fig. 8) all drop off from threshold just as in the nonrelativistic case.[20] For p waves, however, the relativistic interactions contract the wave functions with the result that the relativistic phase shifts are all larger than the nonrelativistic as discussed above.

B. Photoionization cross sections

The photoionization cross section for a given subshell is the sum of partial cross sections corresponding to alternate continuum waves. The relative contribution of alternate partial waves differ in the various energy ranges. Thus for a full understanding of photoionization cross sections, we start our discussion with partial cross sections.

In Fig. 9 the partial cross sections corresponding to

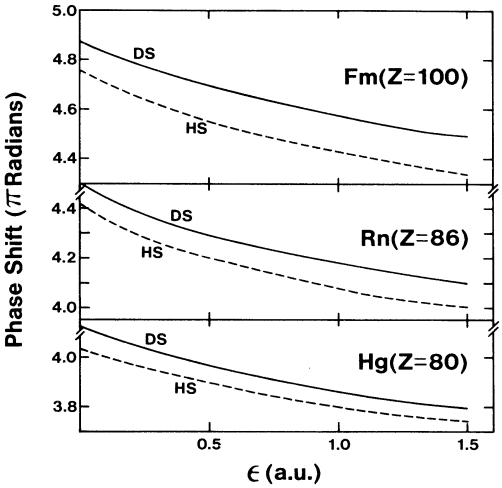

FIG. 8. Phase shifts, in units of π radians, of $p_{1/2}$ continua for Hg ($Z=80$) Rn ($Z=86$), and Fm ($Z=100$) which arise in $5d$ photoionization. The solid curves are the present DS results and the dashed curves are the HS results for the nonrelativistic p relativistic p continuum.

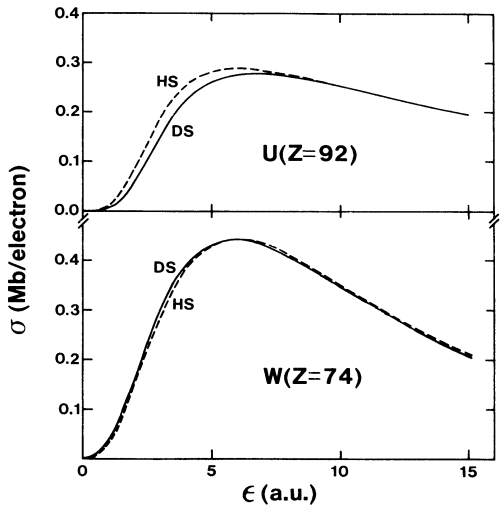

FIG. 9. Photoionization cross section *per electron* for the $4f_{5/2} \rightarrow \epsilon g_{7/2}$ transition in W ($Z=74$) and U ($Z=92$). The solid curves are the present DS results and the dashed curves are the nonrelativistic HS $4f \rightarrow \epsilon g$ results.

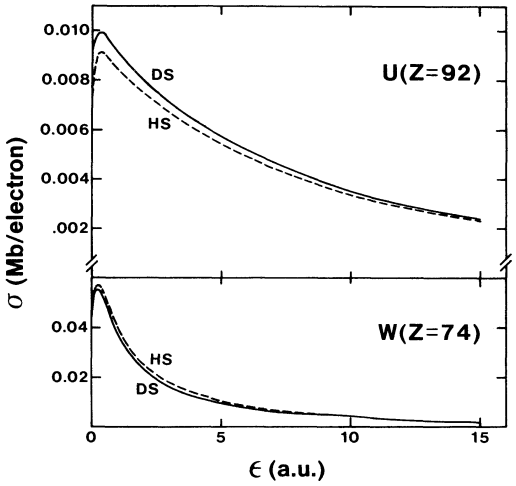

FIG. 10. Photoionization cross section *per electron* for the $4f_{5/2} \rightarrow \epsilon d_{3/2}$ transition in W ($Z=74$) and U ($Z=92$). The solid curves are the present DS results and the dashed curves are the nonrelativistic HS $4f \rightarrow \epsilon d$ results.

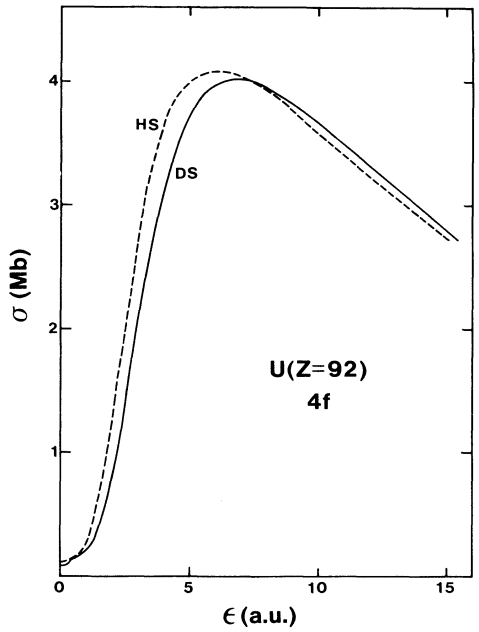

FIG. 11. Total $4f$ photoionization cross section for U ($Z=92$). The solid curve is the DS result and the dashed curve is the nonrelativistic HS result.

$4f \rightarrow \epsilon g$ transition are shown for W ($Z=74$) and U ($Z=92$) in both the HS and DS approximations. The cross sections are per electron in the subshell and only the relativistic $4f_{5/2} \rightarrow \epsilon g_{7/2}$ is shown. Note that the cross sections show no major differences, as Z increases, due to the absence of a bound g state in this range of Z. The delayed maximum is a result of the centrifugal barrier for the g electrons. The small differences between DS and HS cross sections are due to the combined effects of the continuum wave function being "pushed out" by relativistic effects, as discussed above, and the same happening to the discrete $4f$ wave functions.

In Fig. 10 the partial cross sections for $4f \rightarrow \epsilon d$ transitions are shown. These cross sections are large at the threshold compared to the $f \rightarrow g$ transitions, but small away from threshold. Thus the g waves make a dominant contribution at higher energy while the d waves predominate near threshold. The difference between HS and DS results is quite small for $Z=74$ but somewhat larger for $Z=92$. This is to be expected for high-Z elements. In going from $_{74}$W to $_{92}$U, the $4f \rightarrow d$ cross section changes by almost an order of magnitude, resulting from the $6d$ becoming bound in the ground state, so that more and more of the oscillator strength moves into the discrete with increasing Z. It should be noted, however, that the overall agreement between HS and DS calculations is quite good for all of these cases.

Adding up all of the contributions to get the total $4f$ photoionization cross sections, Fig. 11 shows a comparison of the HS and DS results for uranium. It is now straightforward to understand the various features of these results based upon the discussion of the partial cross sections above. The agreement of DS and HS cross sections is excellent, even for so high a Z. It is thus clear that relativistic effects do not significantly alter $4f$ photoionization cross sections; the differences are still smaller for lower Z and only slightly larger for higher Z.

A comparison of the $4f_{7/2}$ the $4f_{5/2}$ cross sections is shown in Fig. 12 for uranium, an element sufficiently heavy so that the effects of the spin-orbit interaction are as large as they are going to be. The relative shapes of these curves are very important in determining the branching ratio for the $4f$ subshell. We see that the two curves almost overlap each other (unlike the $5d$ subshell, as we shall see) indicating that the relativistic interactions do not alter the initial or final states significantly in $4f$ photoionization.

In Fig. 13 the $4f_{5/2}$ cross section for $_{74}$W, $_{80}$Hg, and $_{92}$U is shown. It is seen that the cross sections do not change a great deal in going from tungsten to uranium. At threshold, where the $f \rightarrow d$ transition dominates, the relative difference is much larger due to the large changes

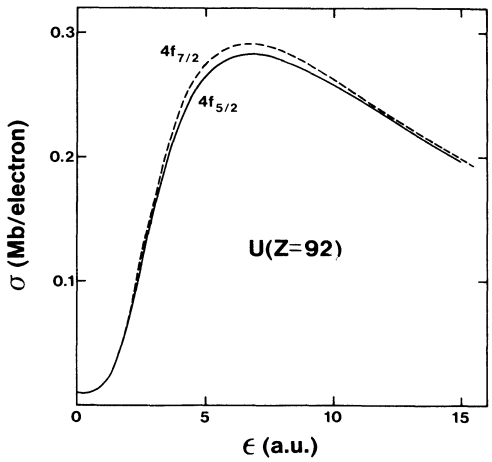

FIG. 12. Photoionization cross section *per electron* for $4f_{7/2}$ and $4f_{5/2}$ in U ($Z=92$).

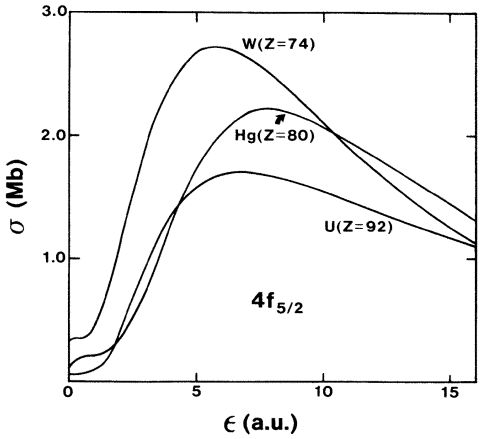

FIG. 13. Total $4f$ photoionization cross sections for W ($Z=74$), Hg ($Z=80$), and U ($Z=92$).

in the d-wave cross sections as we approach the next d bound state. The higher-energy cross sections change much less because there is no bound g state. An overall trend of the maximum in the cross section becoming lower and broader with increasing Z is seen. The systematics of the $4f_{7/2}$ cross section are exactly the same.

The cross sections for the photoionization of $5d$ subshells are much more complicated than for the $4f$. To illustrate, the $5d_{3/2}\rightarrow\epsilon f_{5/2}$ DS cross sections (per electron) are shown in Fig. 14 in the threshold region along with the HS results. For $_{80}$Hg, the HS cross section has a maximum which is somewhat higher and at somewhat lower

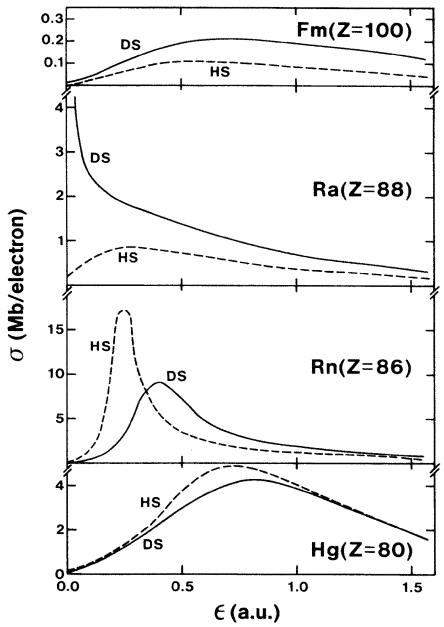

FIG. 14. Photoionization cross section *per electron* for the $5d_{3/2}\rightarrow\epsilon f_{5/2}$ transition in Hg ($Z=80$), Rn ($Z=86$), Ra ($Z=88$), and Fm ($Z=100$). The solid curves are the present DS results and the dashed curves are the nonrelativistic HS $5d\rightarrow\epsilon f$ results.

energy than the DS result; this is entirely consistent with the fact that the f-wave phase shifts are somewhat larger in HS compared to DS as discussed above (Fig. 7). Going up in Z to $_{86}$Rn, the HS peak is at significantly lower energy, almost a factor of 2 larger, and considerably narrower than the DS peak. This clearly indicates that the barrier in the f-wave potential is lower and narrower for HS than for DS, an indication borne out by the phase shifts; it is seen from Fig. 7 that the rise in the HS phase shift is much more rapid and at lower energy than the DS.

Going further up in Z to $_{88}$Ra, Fig. 14 shows that the HS and DS cross sections are completely different near threshold. The DS cross section is dropping from threshold and its maximum value is about a factor of 2 smaller than the $_{86}$Rn case; the HS cross section rises somewhat from threshold and its maximum is smaller by a factor of almost 20 than the $_{86}$Rn case. Clearly something is going on between $Z=86$ (Rn) and $Z=88$ (Ra). The something is the potential now being sufficiently strong to come close to binding a $5f$ electron in the ground state. This is clearly indicated by the f-wave phase shifts in Fig. 7. Instead of the threshold values being about π, as they are for $_{86}$Rn, they are close to 2π for $_{88}$Ra. The difference in f-wave phase shifts between HS and DS in this case is crucial. For the HS result, the ϵf wave function has moved in by one full node at threshold as compared to $_{86}$Rn, i.e., another lobe of the threshold ϵf wave function has moved into the inner well of the effective f-wave HS potential. Thus a large part of the oscillator strength moves into the discrete, leaving the photoionization cross section much smaller. For the DS, on the other hand, the smaller phase shift indicates that the $\epsilon f_{5/2}$ wave function is not in quite as far at threshold. Thus the maximum, seen in the $_{86}$Rn case, moves just into the discrete and the high-energy tail of the cross section maximum still appears in the continuum. It is the sensitivity in this Z region to the barrier between inner and outer wells in the f-wave potential, then, that causes the striking difference between DS and HS results. Based on these arguments, the $\epsilon f_{7/2}$ in $_{88}$Ra, whose phase shift must be smaller than the $\epsilon f_{5/2}$, should have its maximum in the continuum with substantially the same strength as in $_{86}$Rn. This will be demonstrated below.

Going further up in Z to $_{100}$Fm, the DS and HS cross sections are qualitatively similar with the DS result being somewhat higher. This is due to the fact that we are now above the very sensitive region, both phase shifts being 2π at threshold, and the fact that the HS phase shift is larger, moving more of the oscillator strength into the discrete.

Before leaving this discussion two notes are in order. First is that in the sensitive region, the results presented above could be modified substantially in a more accurate calculation, i.e., the results are sensitive to small potential changes. Second is that we have shown only the DS $5d_{3/2}\rightarrow\epsilon f_{5/2}$ results for simplicity but it is clear that the same arguments apply to the other DS $5d\rightarrow f$ transitions and the cross sections for these other transitions are qualitatively similar to those presented above.

Turning our attention to the $d\rightarrow p$ transitions, the $5d_{3/2}\rightarrow\epsilon p_{1/2}$ cross sections (per electron) are shown in Fig. 15 along with the HS results. Agreement is quite good in all cases with the HS being larger than the DS in

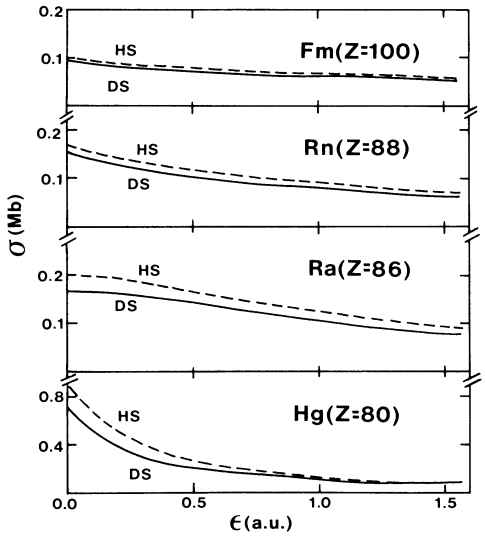

FIG. 15. Photoionization cross section *per electron* for the $5d_{3/2} \rightarrow \epsilon p_{1/2}$ transition in Hg ($Z=80$), Rn ($Z=86$), Ra ($Z=88$), and Fm ($Z=100$). The solid curves are the present DS results and the dashed curves are the nonrelativistic HS $5d \rightarrow \epsilon p$ results.

all cases as well. This is because, as discussed previously (Fig. 8), the DS phase shifts are larger than the HS for p waves so that more of the DS oscillator strength is in the discrete compared to HS. Further, with increasing Z, more and more oscillator strength moves into the discrete region.

The total $5d_{3/2}$ photoionization cross sections (per electron), sums of the $5d_{3/2}$ partial cross sections discussed above, are shown in Fig. 16 for three cases. It is clear from the preceding discussion that, with increasing Z, oscillator strength moves into the discrete for both $d \rightarrow f$ and $d \rightarrow p$ transitions, thus resulting in a decrease of the cross section with Z as is seen in Fig. 16. The peak of the cross section, which generally occurs above threshold owing to the f-wave barrier, does not move monotonically but in a complicated fashion reflecting the relative positions of the $5d_{3/2}$ initial state and $\epsilon f_{5/2}$ final state. Note further that just at threshold, the total is virtually all $d \rightarrow p$, while near the maximum it is nearly all $d \rightarrow f$.

The total $5d$ DS cross sections are shown in Fig. 17 for three atoms along with a comparison with the HS result. For $_{80}$Hg, the agreement between the two is quite good over the range shown, the largest differences occurring at very low energies between the $5d_{5/2}$ and $5d_{3/2}$ thresholds. The splitting of the thresholds is, however, small in this case. Going up in Z, to $_{88}$Ra, the situation is completely different. Aside from the spin-orbit splitting of the thresholds, the shape of the DS curve is quite different from the HS. The $5d_{3/2}$ cross section drops from threshold, as discussed above; the $5d_{5/2}$ has a major delayed maximum which has not yet moved into the discrete. This latter effect is due to the fact that the $5d_{5/2} \rightarrow \epsilon f_{7/2}$ transition is the major contributor to the $5d_{5/2}$ cross section and since $\delta_{f_{7/2}} < \delta_{f_{5/2}}$ (discussed above), the $5d_{5/2}$ maximum is moved out far enough to be above threshold.

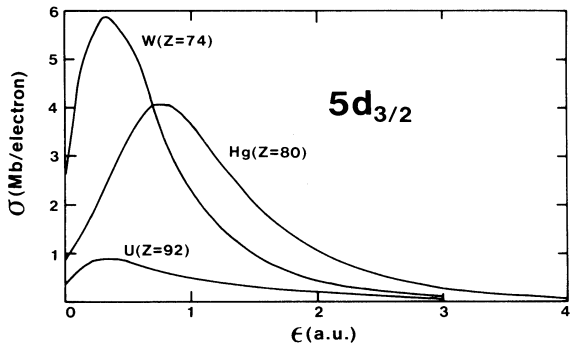

FIG. 16. Photoionization cross section *per electron* for the $5d_{3/2}$ subshell of W ($Z=74$), Hg ($Z=80$), and U ($Z=92$).

Going further up in Z to $_{100}$Fm, we again get significant differences between DS and HS results, partially due to the splitting of the thresholds and partially due to the magnitude of the DS cross sections as discussed above in connection with Fig. 14.

Up to this point, we have concentrated on the near threshold behavior of the cross sections. At higher energies, well above the cross section maximum near threshold, all of these cases exhibit a change of sign in the $d \rightarrow f$ dipole matrix elements, i.e., each has a zero known as a Cooper minimum.[22] To illustrate this, the $5d_{3/2}$ cross section in W is shown in Fig. 18 along with the HS result. Both cross sections are seen to have a Cooper minimum in the range between 5 and 10 a.u. with the HS minimum somewhat lower in energy than the DS. Note that the minimum in the cross section is not exactly where the

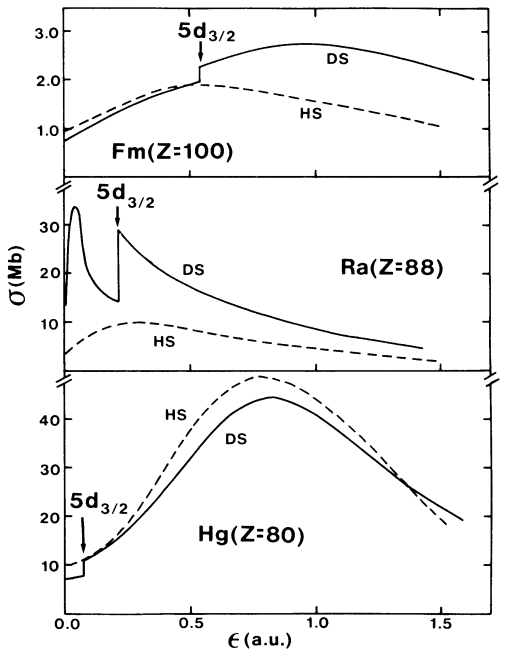

FIG. 17. Total $5d$ photoionization cross sections for Hg ($Z=80$), Ra ($Z=88$), and Fm ($Z=100$). The solid curves are the present DS results and the dashed curves are the nonrelativistic HS results.

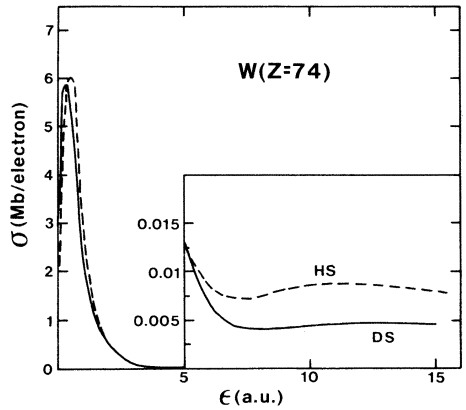

FIG. 18. Photoionization cross section *per electron* for the $5d_{3/2}$ subshell of W ($Z=74$) showing an enlargement of the high-energy region (note change of both scales). The solid curve is the DS result and the dashed curve is the nonrelativistic HS result.

Cooper minimum occurs because the $d\rightarrow p$ cross sections are decreasing in both cases thus causing the minima in the total cross sections to lie at a somewhat higher energy than the energy at which the $d\rightarrow f$ matrix elements vanish.

Note further that the agreement between the HS and DS results is quite good in the low-energy region, well below the Cooper minima, but at higher energies the difference between the positions and shapes of the minima causing significant (factor of 2) differences between the two cross sections. The cross sections are thus seen to be sensitive functions of the details of the Cooper minima. Further discussion of the Cooper minima is given in the next section.

It was seen in the discussion of the $4f$ subshell above that the $4f_{5/2}$ and $4f_{7/2}$ cross sections per electron came very close to overlapping when compared versus photoelectron energy with the consequence that differences in the shapes of the two were not important considerations in the determination of the branching ratio. For $5d$ photoionization, the situation is somewhat different. For $_{92}$U, the $5d_{3/2}$ and $5d_{5/2}$ cross sections per electron are compared in Fig. 19 in the low-energy region. From this curve, it is seen that the shapes are very similar. At higher energies, however, in the Cooper minimum region, significant differences between the two are found to exist, as shall be discussed in the next section. Further, looking back at Fig. 17 for the total cross sections, it is seen that good agreement in shape between $5d_{3/2}$ and $5d_{5/2}$ is in evidence for both $_{80}$Hg and $_{100}$Fm in the low-energy region. The situation for $_{88}$Ra is radically different, for reasons discussed previously, and the difference in these shapes translates to significant dynamical effects in the branching ratio.

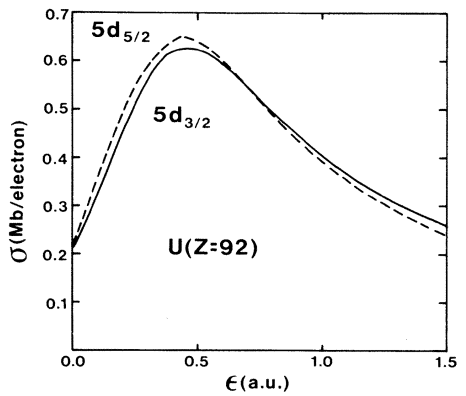

FIG. 19. Photoionization cross section *per electron* for $5d_{5/2}$ and $5d_{3/2}$ in U ($Z=92$).

C. Cooper minima

It is well known that the $5d$ orbital has a zero in the $5d\rightarrow\epsilon f$ channel in the HS calculation.[23] In the neighborhood of this minimum the cross section is much lower since the f wave makes the dominant contribution to the cross section in the high-energy region. The existence and location of this minimum also has important consequences for the angular distribution asymmetry parameter.

The $5d\rightarrow\epsilon f$ channel of a nonrelativistic calculation is split into three separate channels in a relativistic treatment. The $5d$ subshell is split into $5d_{3/2}$ and $5d_{5/2}$ components due to the spin-orbit interaction and the ϵf continuum wave is split into $\epsilon f_{5/2}$ and $\epsilon f_{7/2}$ components. Of these the transition $5d_{3/2}\rightarrow\epsilon f_{7/2}$ is not allowed because of the selection rule $\Delta j=0,\pm 1$. Thus we have three possibilities. These are $5d_{3/2}\rightarrow\epsilon f_{5/2}$, $5d_{5/2}\rightarrow\epsilon_b 5/2$, and $5d_{5/2}\rightarrow\epsilon f_{7/2}$. As a result we can expect one Cooper minimum in the cross section curve for $5d_{3/2}$ and two minima in the $5d_{5/2}$ cross section, one for each of the $d\rightarrow f$ transitions. Note that for $6p$ photoionization, it has been found that relativistic interactions give rise to both a significant splitting and shift of these zeros from the nonrelativistic location.[8,9]

Of the two minima $5d_{5/2}\rightarrow\epsilon f_{5/2},\epsilon f_{7/2}$, the $\epsilon f_{5/2}$ minimum will occur at a lower energy. This comes about since the spin-orbit interaction is attractive for $f_{5/2}$ and repulsive for $f_{7/2}$, thus having the effect of increasing the phase shifts for $\epsilon f_{5/2}$ and decreasing them for $\epsilon f_{7/2}$. Increased phase shifts imply a wave function which is pulled in toward the nucleus. Thus, since continuum wave functions move in with increasing energy, the one with the larger phase shift will reach the point of zero dipole matrix element at a lower energy. Further, it is clear that $5d_{3/2}\rightarrow f_{5/2}$ minimum will occur at a much higher energy than $5d_{5/2}\rightarrow f_{5/2}$. The $5d_{3/2}$ is a more compact bound state and hence the $f_{5/2}$ must be "pulled in" more than for the $5d_{5/2}$ component, hence higher energy for the $5d_{3/2}\rightarrow\epsilon f_{5/2}$ minimum. Thus the $5d_{5/2}\rightarrow\epsilon f_{5/2}$ will occur at the lowest energy. The other two minima ($5d_{3/2}\rightarrow\epsilon f_{5/2}$, $5d_{5/2}\rightarrow\epsilon f_{7/2}$) present a more difficult challenge. Both $d_{3/2}$ and $f_{5/2}$ are "pulled in" while $d_{5/2}$ and $f_{7/2}$ are "pushed out." If the increase in quantum defect in going from $5d_{5/2}\rightarrow 5d_{3/2}$ overcomes the increase in phase shift in going from $\epsilon f_{5/2}$ to $\epsilon f_{7/2}$, then the $5d_{3/2}\rightarrow\epsilon f_{5/2}$ zero will occur at the highest energy. This is what actually does happen because the spin-orbit effect on d states is larger than on f states so that the shift of the $5d$ states dominates. The nonrelativistic HS zero will

be at the lowest energy, lower than *any* of the relativistic, because the HS f-wave phase shift is larger than the relativistic.

The trajectories of these zeros, as a function of Z, are shown in Fig. 20, where it is seen that the ordering of the zeros is as discussed above, independent of Z. The striking things about these results are the sizes of the splittings, between the minima for a given Z, and the structure as a function of Z. The splitting between the $5d_{5/2}\rightarrow\epsilon f_{5/2}$ and $5d_{3/2}\rightarrow\epsilon f_{5/2}$ zeros in Hg is about 0.75 a.u. and in Fm about 1.5 a.u. as compared to the spin-orbit splittings in the $5d$ states of about 0.09 and 0.25 a.u., respectively. Thus the splittings of the zeros is almost an order of magnitude larger than the discrete energy splittings. This is exactly what was found for $6p$ photoionization[8] and the reasons are discussed in detail in Ref. 8.

Briefly, a given amount of energy, the discrete spin-orbit splitting, is required to pull the $5d_{5/2}$ wave function in to the $5d_{3/2}$. The same amount of energy is *not* enough to move the ϵf wave function the same distance in, in the same region of space, owing to the centrifugal barrier. This barrier is much larger for f waves than for d waves so that much more energy is required to move an f wave in a certain distance than a d wave. This "magnification" is, thus, due to the centrifugal barrier.

The splittings increase, as a function of Z, owing to the increasing strength of the spin-orbit interaction. The structure in the trajectories of the zeros, as a function of Z, is yet to be explained. Basically, as discussed above, the energy at which a zero occurs is dependent upon the relative positions of the discrete d- and continuum f-wave functions. Below $Z=80$, the $5d$ shell is still filling and the $5d$ wave functions are contracting with increasing Z; the ϵf wave function remains pretty much the same, its phase shift at threshold staying at π and the slow increase above threshold not changing very much with Z (cf. Fig. 7). Thus it takes more and more energy to move the ϵf functions far enough in for the matrix element to vanish. Above $Z=80$, the $5d$ functions are still contracting with Z, but the ϵf's undergo a dramatic contraction (a shape resonance) just above threshold, as seen in Fig. 7 for $Z=86$. This latter contraction intensifies with increasing Z so that the zero moves to lower energies. In fact, above $Z=86$, Fig. 7 shows that the f-wave phase shifts are 2π at threshold, thus demonstrating the further contraction of the ϵf functions and results in the change of slope seen in Fig. 20 just above $Z=86$.

This behavior persists until $Z=90$, above which the position of the zeros oscillates with increasing Z. The oscillation is small ($\sim$0.2 a.u.) but real and comes about because of the irregular filling of the $6d$ shell as compared to the $5f$. For example, the outer structure of $Z=90$ is $6d^2$, while for $Z=92$ it is $5f^26d$, for $Z=94$ it is $5f^6$, and for $Z=96$ it is $5f^76d$. This nonmonotonic filling of the shells leads to nonmonotonic potentials near the outer edges of the atoms which in turn leads to the observed structure in a complicated manner. We have confirmed this by performing calculations assuming no $6d$ electrons for any of the atoms; the result was the removal of the structure in the $Z=90$—100 range.

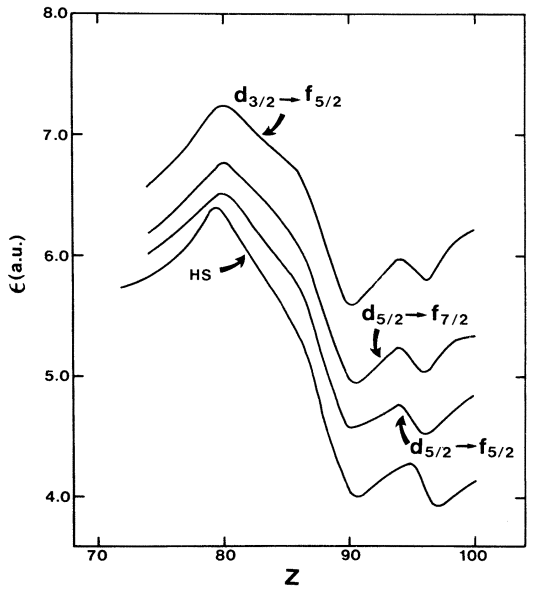

FIG. 20. Trajectory (in photoelectron energy) of the Cooper zeros in the $5d\rightarrow f$ dipole matrix elements as a function of Z.

D. Asymmetry parameter

The asymmetry parameter β, describing the photoelectron angular distribution, is given by Eq. (6). It is seen that β depends not only upon the absolute squares of the transition matrix elements, but also upon their phases. The results for mercury $4f_{7/2}$ are shown in Fig. 21, along with the RRPA results[16] and experiment.[5] The $4f_{5/2}$ result (not shown) is virtually exactly the same as the $4f_{7/2}$, as is the nonrelativistic HS result[24] (not shown). Our DS result is seen to be in good agreement with RRPA and both show excellent agreement with experiment in the low-energy region but only fair agreement at higher energies. This disagreement is not understood.

The small difference between RRPA and DS is due principally to the correct inclusion of exchange in the RRPA calculation. This surmise is made on the basis of a Hartree-Fock (HF) calculation[24] which lies virtually on top of the RRPA result. This is not surprising, as it is known that photoionization channels with a great deal of

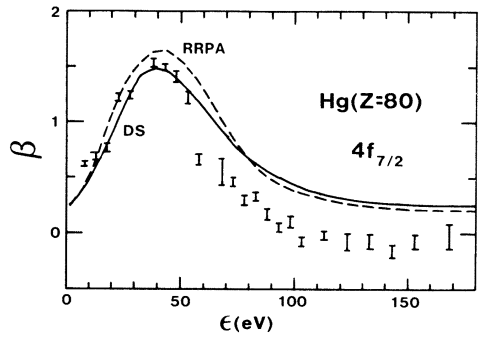

FIG. 21. Photoelectron angular distribution asymmetry parameter β for Hg $4f_{7/2}$. The present DS results (dashed curve) are compared with the RRPA results of Ref. 16 (solid curve) and the experimental points of Ref. 5.

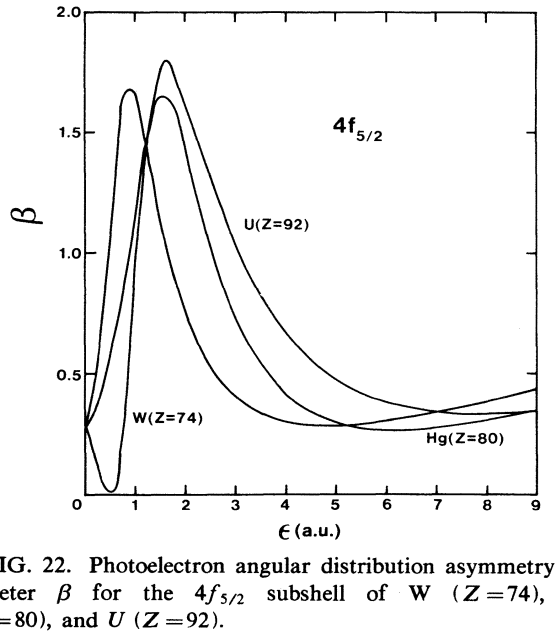

FIG. 22. Photoelectron angular distribution asymmetry parameter β for the $4f_{5/2}$ subshell of W ($Z=74$), Hg ($Z=80$), and U ($Z=92$).

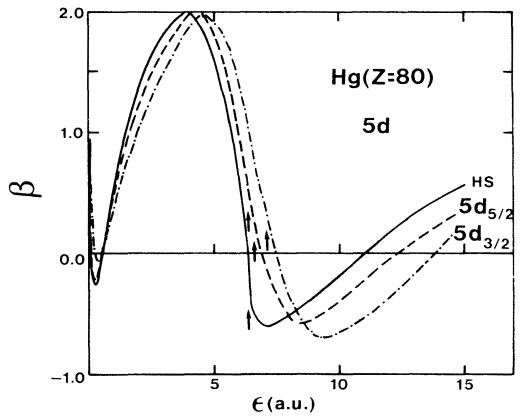

FIG. 24. Photoelectron angular distribution asymmetry parameter β for Hg $5d_{5/2}$ and $5d_{3/2}$, also shown in the nonrelativistic HS $5d$ result. The arrows indicate the locations of the various zeros in the $5d \rightarrow f$ dipole matrix elements.

oscillator strength (such as the $4f$ in Hg) are not much affected by interchannel coupling.

The general shape of the variation of β with energy can be understood by recalling that the mercury $4f$ cross section is dominated by the $4f \rightarrow \epsilon d$ transition near threshold, while at higher energies the $4f \rightarrow \epsilon g$ dominate; in the intermediate region they are comparable. If we assume the $4f \rightarrow \epsilon g$ matrix elements vanish at threshold, then Eq. (6) gives a β of about 0.29, which is very close to what is seen in Fig. 21. In the higher-energy region, the flat plateau of β of about 0.2 can be explained by looking at Eq. (6). If we assume *no* relativistic differences among matrix elements and phases for continuua of a given l, we get

$$\beta = \tfrac{5}{7}(1 - \tfrac{18}{5}\rho \cos\Delta) , \qquad (7)$$

where ρ ($\ll 1$) is the ratio of the $4f \rightarrow \epsilon d$ to $4f \rightarrow \epsilon g$ matrix elements, Δ is the total g-d phase-shift difference, and terms of order ρ^2 are neglected. Then, noting that $\cos\Delta \approx 1$ in this region and $\rho \approx \frac{1}{5}$, Eq. (7) yields a β of about 0.2. The matrix elements and especially the phases are slowly varying in this energy region, thus creating the plateau seen. In the intermediate-energy region, near the peak of the β curve, the matrix elements are about equal; furthermore, the phase shifts are changing fairly rapidly. Thus a fairly rapid change of β with energy is expected and seen in Fig. 21. The fact that β rises, rather than falls, between the two regions is a consequence of the value of the phase difference between d and g waves.

The arguments presented above, which have been made earlier in connection with the nonrelativistic calculation,[24] are not specific to mercury and should be generally true for other $4f$ β's in high-Z elements. In Fig. 22 our β values for $4f_{5/2}$ photoionization in W ($Z=74$), Hg ($Z=80$), and U ($Z=92$) are shown and they are very similar. At threshold they all go to about the same values, in the intermediate region they all rise to a value near 2, and at higher energies they all plateau at a low value of β.

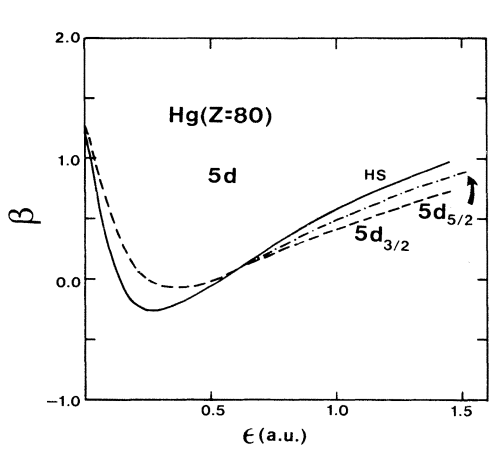

FIG. 23. Photoelectron angular distribution asymmetry parameter β, for Hg $5d_{5/2}$ and $5d_{3/2}$, also shown in the nonrelativistic HS $5d$ result.

The situation for the $5d$ subshell is more complicated and the β parameters have more structure as a function of energy as was seen in Figs. 3 and 4 for mercury. It was also seen that, in that case, excellent agreement with experiment was obtained. In Fig. 23 a comparison of DS and HS β's are shown for mercury $5d$ in the low-energy region. In the very low-energy region, the $5d_{5/2}$ just about coincides with the HS results while the $5d_{3/2}$ is shifted outward a bit. At somewhat higher energies, the HS is shifted inward from the $5d_{5/2}$. At still higher energies, shown in Fig. 24, the curves show roughly the same general shape, HS being the innermost and $5p_{3/2}$ being the outermost. That the HS is the innermost curve is a consequence of the f-wave phase shift being the largest in this case, as discussed earlier in connection with the cross sections. The ordering of the $5d_{3/2}$ and $5d_{5/2}$ curves is a consequence of the $j=\frac{5}{2}$ being more diffuse than the $j=\frac{3}{2}$ state, just as was seen for the cross sections.

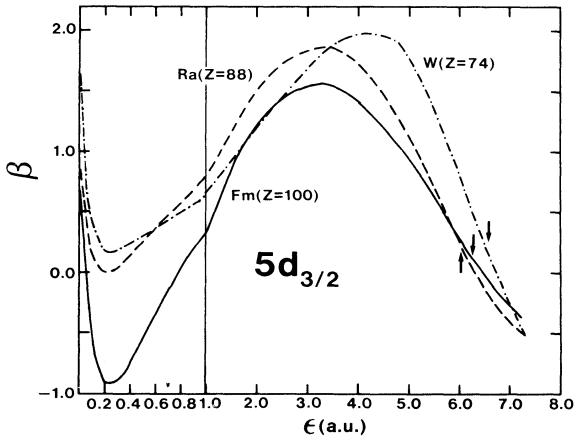

FIG. 25. Photoelectron angular distribution asymmetry parameter β for the $5d_{3/2}$ subshell of W ($Z=74$), Ra ($Z=86$), and Fm ($Z=100$). Note the change of horizontal scale at 1 a.u. The arrows indicate the locations of the various zeros in the $5d \rightarrow f$ dipole matrix elements.

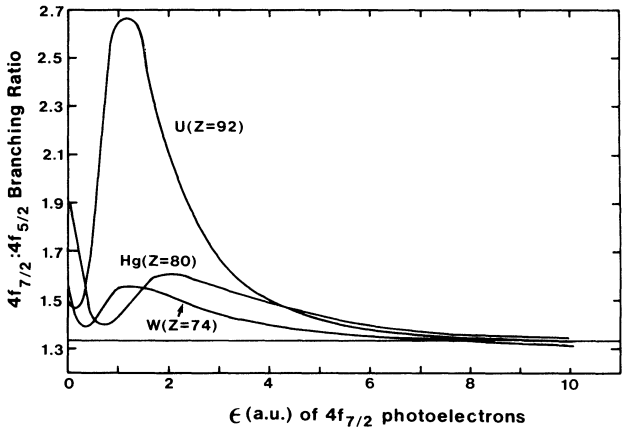

FIG. 26. $4f_{7/2}:4f_{5/2}$ branching ratios for W ($Z=74$), Hg ($Z=80$), and U ($Z=92$). The solid line at 1.33 is the statistical ratio.

This splitting of the β's increases with increasing energy as seen in Fig. 24. The splitting around 7 a.u. reflects the splitting of the Cooper minima (cf. Fig. 20) which is about 0.5 a.u. for mercury. From Fig. 20, it is clear that the splitting of the Cooper minima increases with increasing Z; thus for higher Z the splitting of the β's for the two spin-orbit components also increases.

The general shape of the β curves is typical of a d state with a Cooper minimum.[25] They are determined largely by three factors. At the lowest energies the rapid drop from the threshold value is caused by the rapid variation in the Coulomb phase shifts. The following broad maximum is a result of the shape resonance in the $d \rightarrow f$ channels. The rapid drop at still higher energies is a consequence of the change in sign of the $d \rightarrow f$ matrix elements, i.e., the Cooper minima.

The results for several $5d_{3/2}$ β's are shown in Fig. 25 from which it is clear that all of the $5d$ β's have this same general shape. Of course there are differences in detail owing to changing matrix element ratios, phase-shift differences, and Cooper minima locations, with increasing Z. These, however do not affect the overall systematics. The $5d_{5/2}$ β's (not shown) have all of the same features as the $5d_{3/2}$ but the curves are compressed somewhat as discussed above.

Before leaving the discussion of photoelectron angular distributions it is important to mention that, for high-Z elements particularly, contributions to the angular distribution can come not only from the electric dipole term (which we have considered) but from higher multipoles as well.[26,27] Of course this is very important at high energies (tens of kilo-electron-volts) but, even at low energies, if the dipole cross section is small, e.g., in a Cooper minimum region, the higher multipoles can give an effect of the order of 10%. This can be important as measurements get more and more precise.

E. Branching ratios

As discussed in the Introduction, the branching ratio $\sigma(j=l+\frac{1}{2})/\sigma(j=l-\frac{1}{2})$ differs from the statistical value of $(l+1)/l$ only because of relativistic interactions. These manifest themselves in two distinct ways. The spin-orbit splitting of the bound state energies means that the photoelectrons will have different kinetic energies for the same $h\nu$. Thus, even if each of the cross sections are exactly the same as a function of photoelectron energy, the spin-orbit splitting gives rise to a nonstatistical branching ratio. This is known as the kinetic energy effect.[6] In addition, the shapes of the individual cross sections can differ owing to dynamical effects on the wave functions, thus further causing deviations from the statistical ratio.

It is, therefore, clear that branching ratios spotlight relativistic effects. In addition, comparison with experiment is very useful because branching ratio measurements do not require normalized cross sections, which removes a possible source of error from the measurement.

A selection of our $4f$ branching ratios is given in Fig. 26 where we see, in each case, a drop from threshold followed by a rise to a maximum, and then a tailoff to the statistical value of 1.33 at high energy. Further, the max-

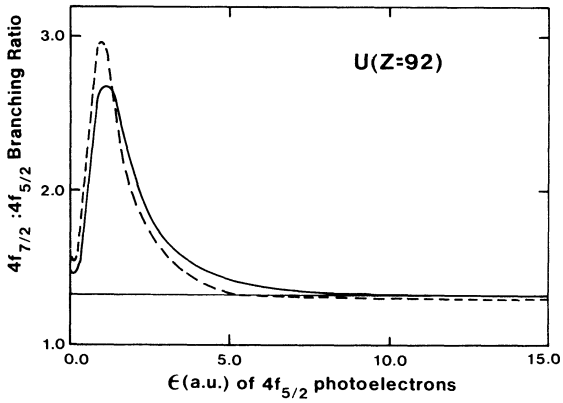

FIG. 27. $4f_{7/2}:4f_{5/2}$ branching ratio for U ($Z=92$). The solid curve is the present DS result and the dashed curve is derived by applying the kinetic energy effect to the nonrelativistic HS cross section. See text for details.

imum is seen to become more pronounced with increasing Z. This behavior can be understood by noting that there are very few dynamical effects in the $4f$ shell as exemplified in Fig. 12 for the $4f_{7/2}$ and $4f_{5/2}$ cross sections of uranium. Thus the kinetic energy effect dominates and increases with increasing Z where the discrete spin-orbit splitting increases.

To show this more clearly, we have done an approximate calculation of the branching ratio in uranium assuming that the cross sections per electron for $4f_{5/2}$ and $4f_{7/2}$ were each the nonrelativistic HS result. The results are given in Fig. 27 where it is seen that the approximate calculation is in excellent agreement with the actual results. The only real difference occurs around the maximum in the curve, owing to a small amount of dynamical differences in the cross sections as seen in Fig. 12. This result is indicative of all of the high-Z $4f$ cases which we have investigated.

The situation for the $5d$ subshell is somewhat different because of the significant dynamical effects on the cross section, as discussed in Sec. III B, and because of the Cooper minima. The results for a number of cases are given in Fig. 28. The overall behavior of each of the branching ratios is a drop from a large threshold value followed by a broad region where the branching ratio is below the statistical value, followed by a rise above the statistical value. The behavior away from the threshold is easy to understand. The zero in the $d_{5/2}\rightarrow f$ dipole matrix elements occurs at lower energies than the corresponding $d_{3/2}\rightarrow f$ matrix element. Thus at the energies in the vicinity of the $d_{5/2}$ zeros, the $5d_{5/2}$ cross section is anomalously small. It follows then, that in this region the branching ratio will also be smaller than the statistical value. At higher energies where the $5d_{3/2}$ has its zero, the $5d_{3/2}$ cross section is anomalously small and the reverse occurs; the branching ratio climbs above the statistical value. The behavior near threshold is largely due to the kinetic energy effect, for the cases shown, although dynamical effects do play a role in the details of the drop off.

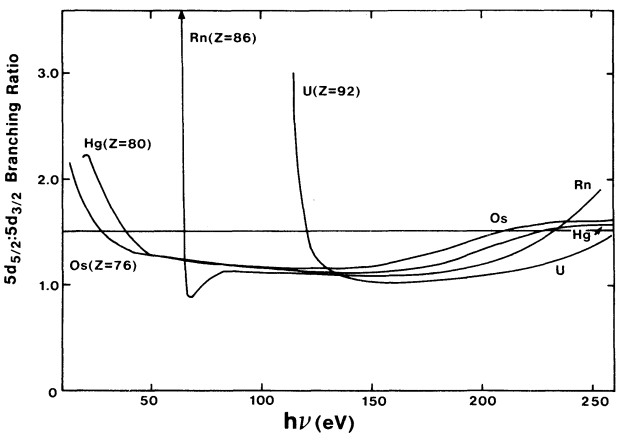

FIG. 28. $5d_{5/2}$:$5d_{3/2}$ branching ratios for Os ($Z=76$), Hg ($Z=80$), Rn ($Z=86$), and U ($Z=92$). The solid line at 1.5 is the statistical ratio.

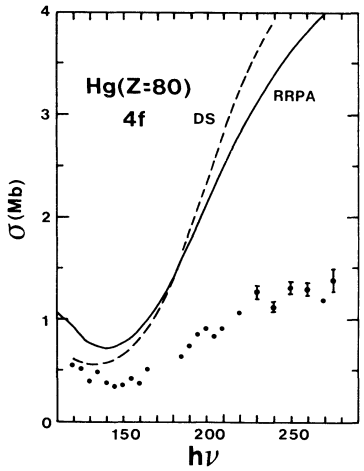

FIG. 29. Total $4f$ photoionization cross section for Hg ($Z=80$). The dashed curve is the present DS result, the solid curve is the RRPA result of Ref. 16, and the experimental points are from Ref. 5.

IV. FINAL REMARKS

The effects of relativistic interactions on $4f$ and $5d$ subshells of high-Z elements have been examined. We have found considerable splitting of the Cooper minima of the $5d\rightarrow\epsilon f$ transitions for a given element, similar to the $6p\rightarrow\epsilon d$ case studied previously.[8,9] This, in turn, affected the photoelectron angular distributions and branching ratios. Furthermore, significant *dynamical* differences in the cross sections of $5d_{5/2}$ and $5d_{3/2}$ were found, apart from the shift in thresholds. For $4f$ photoionization, on the other hand, relativistic interactions were found to have almost no effect on the cross sections, except for the splitting of $4f_{7/2}$ and $4f_{5/2}$ thresholds; the shapes of the $4f_{7/2}$ and $4f_{5/2}$ cross sections were found to be virtually the same as each other and the nonrelativistic result. Thus the variation of the branching ratio could be explained by the "kinetic energy effect."

One problem exists with $4f$ photoionization, however. While the branching ratios and photoelectron angular distribution β parameters are in reasonable agreement with experiment for mercury, the cross section is not.[5] The comparison, shown in Fig. 29 along with the RRPA result[16] shows discrepancies of more than a factor of 2 at the highest energies measured; the experimental value is below 1.5 Mb while both DS and RRPA are above 4 Mb. This difference is quite surprising in view of the simplicity of $4f$ photoionization. While there are many inadequacies in the theory, it is hard to see how they could explain so large a discrepancy. On the experimental side, it is possible that there is some error in the normalization of the cross section. In any case, this matter should be studied further.

Finally, we note that relativistic photoionization studies exist where results are analyzed for the various subshells of given elements,[26–28] rather than as a function of Z. These studies provide complementary information to the analysis presented in this paper; they show the evolution of features as a function of a principal quantum number.

ACKNOWLEDGMENTS

The authors would like thank R. H. Pratt, A. Ron, and I. B. Goldberg for valuable discussions concerning this work. We would also like to thank P. H. Kobrin and D. A. Shirley for supplying us with their photoionization data prior to publication. This work was supported by the National Science Foundation.

[1]R. B. Cairns, H. Harrison, and R. I. Schoen, J. Chem. Phys. **53** 96 (1970).
[2]S. Süzer, P. R. Hilton, N. S. Hush, and S. Nordholm, J. Electron Spectrosc. Relat. Phenom. **12**, 357 (1977).
[3]S. P. Shannon and K. Codling, J. Phys. B **11**, 1193 (1978).
[4]G. Schönhense, F. Schafers, U. Heinzmann, and J. Kessler, Z. Phys. A **304**, 31 (1982).
[5]P. H. Kobrin, P. A. Heimann, H. G. Kerkoff, D. W. Lindle, C. M. Truesdale, T. A. Ferrett, U. Becker, and D. A. Shirley, Phys. Rev. A **27**, 3031 (1983).
[6]T. E. H. Walker and J. T. Waber, J. Phys. B **6**, 1165 (1973); **7**, 674 (1974).
[7]B. R. Tambe, W. Ong, and S. T. Manson, Phys. Rev. A **23**, 799 (1981).
[8]S. T. Manson, C. J. Lee, R. H. Pratt, I. B. Goldberg, B. R. Tambe, and A. Ron, Phys. Rev. A **28**, 2885 (1983).
[9]Y. S. Kin, A. Ron, R. H. Pratt, B. R. Tambe, and S. T. Manson, Phys. Rev. Lett. **46**, 1326 (1981).
[10]S. T. Manson, Adv. Electron. Electron Phys. **41**, 73 (1976) and references therein.
[11]D. Liberman, D. T. Cromer, and J. T. Waber, Comput. Phys. Commun. **2**, 107 (1971).
[12]C. N. Yang, Phys. Rev. **74**, 7644 (1948).
[13]F. Keller and F. Combet Farnoux, J. Phys. B **12**, 282 (1979).
[14]H. Harrison, Bull. Am. Phys. Soc. **15**, 514 (1970).
[15]A. Niehaus and M. W. Ruf, Z. Physik **252**, 84 (1972).
[16]W. R. Johnson, V. Radojević, P. Deshmukh, and K. T. Cheng, Phys. Rev. A **25**, 337 (1982).
[17]F. Herman and S. Skillman, *Atomic Structure Calculations* (Prentice-Hall, Englewood Cliffs, N.J., 1963).
[18]H. A. Bethe and E. E. Salpeter, *Quantum Mechanics of One- and Two-Electron Atoms* (Springer, Berlin, 1957), pp. 22 and 72.
[19]J. P. Desclaux and Y. K. Kim, J. Phys. B **8**, 1177 (1975).
[20]S. T. Manson, Phys. Rev. **182**, 97 (1969).
[21]A. R. P. Rau and U. Fano, Phys. Rev. **167**, 7 (1968).
[22]J. W. Cooper, Phys. Rev. **128**, 681 (1962).
[23]S. T. Manson and J. W. Cooper, Phys. Rev. **165**, 126 (1968).
[24]J. S. Shyu and S. T. Manson, Phys. Rev. A **11**, 166 (1975).
[25]D. J. Kennedy and S. T. Manson, Phys. Rev. A **5**, 227 (1972).
[26]H. K. Tseng, R. H. Pratt, S. Yu, and A. Ron, Phys. Rev. A **17**, 1061 (1978).
[27]Y. S. Kim, R. H. Pratt, A. Ron, and H. K. Tseng, Phys. Rev. A **22**, 567 (1980).
[28]A. Ron, Y. S. Kim, and R. H. Pratt, Phys. Rev. A **24**, 1260 (1981).